Can I transform my understanding of **genomics, transcriptomics, and epigenomics** at single cell resolution?

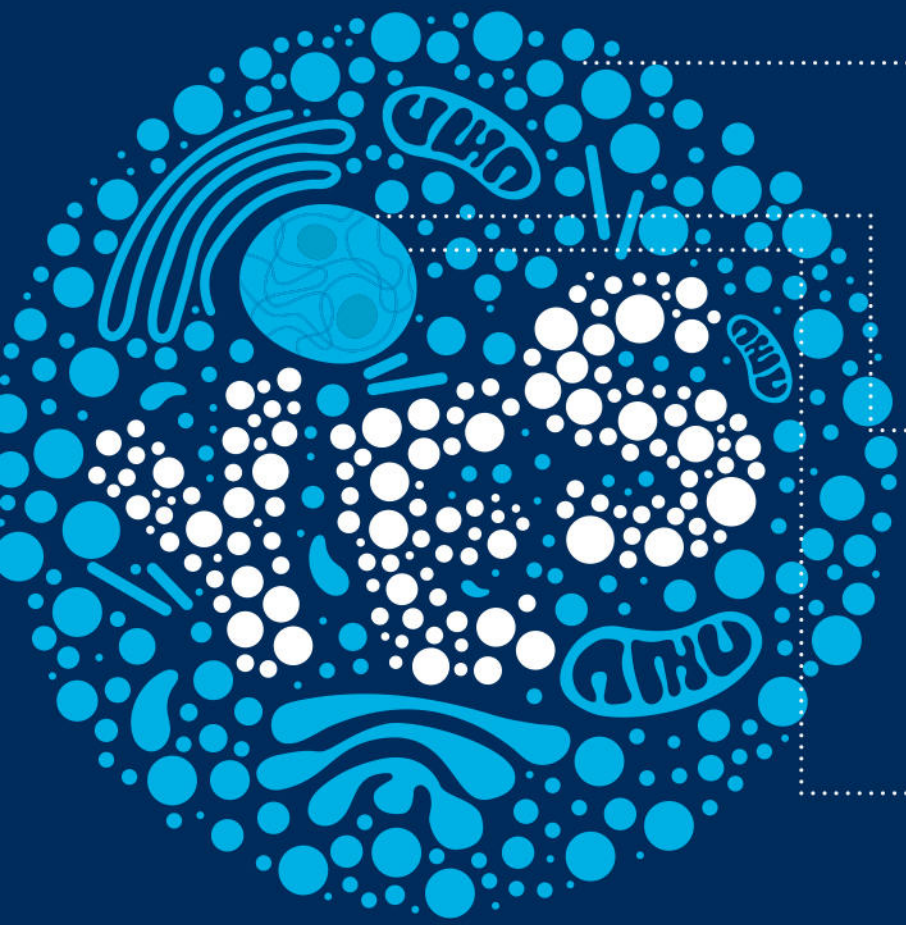

Uncover the full spectrum of cellular diversity and cellular interactions

Unmask true genetic diversity and map clonal evolution in complex disease

Unravel the epigenetic basis of disease and development cell by cell

Get a Multidimensional View of Complex Cellular Systems with Single Cell Solutions from 10x Genomics

Single Cell Transcriptomics

- Gene Expression Profiling
- Gene Expression CRISPR Screening
- Gene Expression & Cell Surface Protein
- Immune Profiling
- Immune Profiling & Cell Surface Protein
- Immune Profiling & Antigen Specificity

Single Cell Genomics

- Copy Number Variation

Single Cell Epigenomics

- Chromatin Accessibility

LEARN MORE AT 10XGENOMICS.COM/YES

10X GENOMICS

STEM CELLS®

TISSUE-SPECIFIC STEM CELLS

Criticality of the Biological and Physical Stimuli Array Inducing Resident Cardiac Stem Cell Determination

GIANCARLO FORTE,[a,b] FELICIA CAROTENUTO,[a] FRANCESCA PAGLIARI,[a] STEFANIA PAGLIARI,[c] PAOLO COSSA,[a] ROBERTA FIACCAVENTO,[a] ARTI AHLUWALIA,[d] GIOVANNI VOZZI,[d] BRUNA VINCI,[d] ANNALUCIA SERAFINO,[e] ANTONIO RINALDI,[f,g] ENRICO TRAVERSA,[f,g] LUCIANA CAROSELLA,[h] MARILENA MINIERI,[a,g] PAOLO DI NARDO[a,g]

[a]Laboratorio di Cardiologia Molecolare e Cellulare, Dipartimento di Medicina Interna, Università di Roma Tor Vergata, Roma, Italy; [b]Istituto Nazionale per le Ricerche Cardiovascolari (INRC), Bologna, Italy; [c]Syntech srl, Roma, Italy; [d]Centro Interdipartimentale di Ricerca "E. Piaggio," Università di Pisa, Pisa, Italy; [e]Istituto di Neurobiologia e Medicina Molecolare, Consiglio Nazionale delle Ricerche, Roma, Italy; [f]Dipartimento di Scienze e Tecnologie Chimiche, Università di Roma Tor Vergata, Roma, Italy; [g]Centro per le Nanoscienze, le Nanotecnologie e la Strumentazione Innovativa (NAST), Università di Roma Tor Vergata, Roma, Italy; [h]Istituto di Medicina Interna e Geriatria, Università Cattolica S. Cuore, Roma, Italy

Key Words. Mesenchymal stem cells • Cardiac progenitor cells • Three-dimensional scaffolds • Tissue engineering

ABSTRACT

The replacement of injured cardiac contractile cells with stem cell-derived functionally efficient cardiomyocytes has been envisaged as the resolutive treatment for degenerative heart diseases. Nevertheless, many technical issues concerning the optimal procedures to differentiate and engraft stem cells remain to be answered before heart cell therapy could be routinely used in clinical practice. So far, most studies have been focused on evaluating the differentiative potential of different growth factors without considering that only the synergistic cooperation of biochemical, topographic, chemical, and physical factors could induce stem cells to adopt the desired phenotype. The present study demonstrates that the differentiation of cardiac progenitor cells to cardiomyocytes does not occur when cells are challenged with soluble growth factors alone, but requires strictly controlled procedures for the isolation of a progenitor cell population and the artifactual recreation of a microenvironment critically featured by a fine-tuned combination of specific biological and physical factors. Indeed, the scaffold geometry and stiffness are crucial in enhancing growth factor differentiative effects on progenitor cells. The exploitation of this concept could be essential in setting up suitable procedures to fabricate functionally efficient engineered tissues. STEM CELLS *2008;26: 2093–2103*

Disclosure of potential conflicts of interest is found at the end of this article.

INTRODUCTION

Novel solutions are needed to circumvent the limited drug efficiency and the shortage of heart donors to treat cardiovascular diseases. Among others, the myocardial inaptitude to self-repair suggested investigating the engraftment of either functionally efficient or stem cell-derived cardiomyocytes [1]. Unfortunately, early clinical trials, aimed at evaluating whether the injection of stem cells [2] could actually improve the function of severely damaged hearts, produced uncertain results [3]. Indeed, further investigations are required to elucidate stem cell biology and other technical steps crucial to clinical practice [4]. Under current protocols, stem cell number and differentiation as well as graft shape, size, and location are unpredictable. Alternatively, tissue engineering techniques [5] allow loading three-dimensional (3D) polymeric matrixes (scaffolds) with committed or differentiated stem cells [6–8] to fabricate bio-substitutes to be engrafted into damaged organs. Actually, encouraging results have been achieved in reconstructing hard tissues, such as bone [9] and cartilage [10], and flat soft tissues, such as cornea [11] and skin [12], whereas more complicated soft tissues, such as the myocardium, are far more challenging to be replicated in vitro. In this context, autologous stem cells are the best candidate to fabricate efficient bio-substitutes because of their multipotency and the capability to elude infectious diseases and host immune response. In vitro, adult mesenchymal stem cells (MSCs) differentiate into adipocytes, chondrocytes, and osteoblasts [13] and commit to cardiomyocytes [14–16]. Recently, adult resident progenitors have been identified in almost all organs [17]. In the mammalian myocardium, tissue-specific precursors (cardiac progenitor cells [CPCs]) preside over cardiac tissue homeostasis [18–21] displaying the ability to generate myocardial phenotypes, such as cardiomyocytes, smooth muscle and endothelial cells [22], and, to a lesser extent, other cell phenotypes [23].

Author contributions: G.F. and F.C.: experimental design and implementation; F.P., S.P., P.C., and R.F.: cell culture; A.A., G.V., and B.V.: polymeric scaffold design and fabrication; A.R. and E.T.: mechanical tests and mathematical model of polymeric scaffolds; A.S. and L.C.: confocal microscopy analysis; M.M. and P.D.N.: study conception and manuscript writing.

Correspondence: Paolo Di Nardo, M.D., Laboratorio di Cardiologia Molecolare e Cellulare, Dipartimento di Medicina Interna, Università di Roma Tor Vergata, Via Montpellier, 1, 00133 Roma, Italy. Telephone: +39-06-72594215; Fax: +39-06-2024130 or +39-06-72594263; e-mail: dinardo@med.uniroma2.it Received January 18, 2008; accepted for publication May 15, 2008; first published online in STEM CELLS *EXPRESS* May 22, 2008. 1066-5099/2008/$30.00/0 doi: 10.1634/stemcells.2008-0061

However, to fabricate engineered tissues, a specific cell population must combine with a scaffold made of appropriately processed polymer materials. A number of polymers have been investigated as tissue engineering scaffolds, including natural compounds (collagen, hyaluronate, chitosan, and fibrin) as well as synthetic polymers, such as polycaprolactone (PCL), polyglicolide (PLGA), polylactide (PLLA), and their copolymers [24]. Synthetic polymers are easier to process [25], mostly using rapid prototyping methods that allow to design layer-by-layer a structure and to control the different phases of its fabrication with a computer-aided design/computer-aided manufacture (CAD/CAM) system. Among others, pressure-assisted microsyringe (PAM) method uses a polymer solution or melt that is extruded through a syringe mounted on an arm or on the z-axis of a 3D micropositioner and allows the fabrication of very finely designed scaffolds [26].

Finally, accurate protocols must be adopted to interface cells and scaffolds maintaining functional cells and regulating cell behavior, while reconstructing 3D tissues. Scaffolds should exhibit biocompatibility and biodegradability [27], high porosity, and adequate pore size to favor cell attachment and growth as well as to facilitate the diffusion of nutrients to and waste products from the construct [28]. Moreover, they should provide physical support to stem cell adhesion, proliferation, and differentiation, and geometrical guidance in tissue organization. The mechanical properties of the scaffold are a further key factor to fit to provide the correct environment for the neotissues. Scaffold mechanics are governed by both materials chemistry and processing methods; nevertheless, little is known about the mechanical properties of many scaffold designs. In fact, since the knowledge of the biological processes remains poor, an unambiguous set of parameters to be assumed a priori when designing a specific scaffold cannot be established yet. Furthermore, the comparative relevance of most of the biochemical, physico-chemical, and mechano-structural signals in determining cell fate has never been exhaustively investigated. Nevertheless, mesenchymal stem cell capability to grow and differentiate on polymeric three-dimensional scaffolds has been related, among others, to the crucial relationship interlacing the stem cell differentiative potential and matrix elasticity [29, 30]. Actually, in most studies, scaffolds have been credited with providing mere physical support for embryonic [31] and mesenchymal stem cell adhesion, proliferation, and differentiation [32], and geometrical guidance in tissue organization, whereas growth factors have been considered as the major players in driving cell differentiation [15, 16]. Therefore, the present study aimed at investigating the potential of different progenitor cell populations cultured on appropriately designed bio-erodable polymeric scaffolds to differentiate to cardiomyocytes. Here, we demonstrate that the fabrication of high-quality myocardial biosubstitutes can be achieved only by supplying stem cells with multiple integrated inputs, among which those provided by scaffolds with fine-tuned mechanical properties are decisive.

MATERIALS AND METHODS

Polymers and Scaffold Microfabrication

The polymers used were PLLA (Lactel Absorbable Polymers, Cupertino, CA, http://www.absorbables.com), PCL (MW 65,000; Sigma-Aldrich, Milano, Italy, http://www.sigmaaldrich.com), PLGA (75:25; Lactel), and a blend of PLLA and PCL (2.5%:20%). All polymers were dissolved in chloroform in the following polymer weight/solvent volume ratios: PLLA 2%, PLGA 20%, and PCL 20%. The PCL/PLLA blend was prepared by mixing equal quantities of 5% PLLA and 40% PCL.

For bidimensional structure fabrication, all polymers were spin-coated onto glass coverslips by applying 0.5 ml of solution and spinning at 400 rpm (SUSS Microtech, Zurich, Switzerland, http://www.suss.com) to obtain thin films of 380-μm height.

PAM system was used to fabricate 3D scaffolds using the polymers that, as films, adequately reacted after challenging with stem cells (PLLA and PLGA). PAM is a microfabrication technique developed and patented by the University of Pisa in which polymer solution is extruded from a microsyringe mounted on a three-axis micropositioner applying a pressure generated by compressed air. The system is interfaced to a personal computer with an inbuilt graphics tool for creating or importing scaffold designs. Scaffold geometry is controlled by modulating the applied pressure and the deposition speed and is also a function of polymer viscosity and syringe diameter. In this study, a simple scaffold topology was selected to mimic the interweaving organization of cardiac tissue. The scaffolds were hexagonal or square grids as shown in Figure 2, with unit sides of 200 μm and line widths of 50 μm, fabricated by depositing three layers. Each layer was laterally offset with respect to adjacent layers by 100 μm.

Scaffold Characterization

Scaffolds and films of PLLA, PLGA, PCL, and PCL/PLLA have been characterized in previous studies [33]. In particular, material contact angles and surface potentials were measured. All materials showed negative surface charge and their hydrophobicity increased in the following order: PCL $<$ PCL/PLLA $<$ PLLA $<$ PLGA. In addition, PAM-produced scaffolds were tested for their stress-strain characteristics as a function of geometry using an isotonic transducer (model 7006; Ugo Basile Biological Research Apparatus, Comerio, Italy, http://www.ugobasile.com), where the applied force had a resolution of 0.001 N. Scaffolds with dimensions of 2 cm length, 0.5 cm width were specifically fabricated for the measurements. The applied force acted along the direction of the maximal length of the structures corresponding to the x-axis of square pores. During the stress-strain tests, the applied weights were changed every 3 minutes, and the Young's modulus of each structure was calculated from the slope of the initial linear portion of the resulting curve. The results are illustrated in Figure 2. Scaffolds were also routinely tested for fidelity by observation with a microscope to ensure that line widths did not vary more than 10% of 50 μm. Samples that did not meet this standard of fidelity, usually due to breakage of the capillary needle during deposition, were rejected.

Mathematical Modeling of Square Scaffold

The local elastic properties in the neighborhood of a square pore is fully described by the compliance matrix $\mathbf{S_M}$ in Voigt notation

$$\mathbf{S_M} = \begin{vmatrix} \frac{1}{E_x} & -\frac{v}{E_x} & 0 \\ -\frac{v}{E_x} & \frac{1}{E_x} & 0 \\ 0 & 0 & \frac{1}{2G} \end{vmatrix} \quad (1)$$

where E_x, v, G are the Young's modulus, the Poisson's ratio, and shear modulus, respectively, measured through mechanical testing and/or simulations along the "material axes" x and y of the square pore. The compliance matrix can be expressed in any other frame of reference x′-y′, rotated by an angle θ from x, through the transformation

$$\mathbf{S}(\theta) = inv(\mathbf{Q}(\theta)[inv(\mathbf{S_M})]\mathbf{Q}^T(\theta)), \quad (2)$$

Where "inv" indicates the inverse matrix operator and $\mathbf{Q}(\theta)$ is defined as

$$\mathbf{Q}(\theta) = \begin{vmatrix} cos^2(\theta) & sin^2(\theta) & cos(\theta)sin(\theta) \\ sin^2(\theta) & cos^2(\theta) & -cos(\theta)sin(\theta) \\ -2cos(\theta)sin(\theta) & 2cos(\theta)sin(\theta) & cos^2(\theta) - sin^2(\theta) \end{vmatrix} \quad (3)$$

The equivalent Young's modulus, defined as $E^*(\theta) = 1/\mathbf{S}_{11}(\theta)$, provides a measure of the stiffness of the structural element in the direction θ. The calculation was implemented in a Matlab (The MathWorks, Inc., Novi, MI, http://www.mathworks.com) script to explore $E^*(\theta)$ on the entire 360° range. The values $\{v, G\}$ to calculate $\mathbf{S}_\mathbf{M}$ and $E^*(\theta)$ were estimated through a numerical model calibrated on the experimental value Ex = 0.35 MegaPascal (MPa) along x and tested in tension and shear.

Scaffold and Film After Treatment

After fabrication, scaffolds and films were washed in water so that they floated off the glass slides and could be handled with tweezers and placed in a dessicator under vacuum for 4–5 days to remove traces of solvent. Before cell seeding, the samples were sterilized with 50% EtOH and under UV light for 15 minutes. Thereafter, scaffolds and films were equilibrated with Dulbecco's modified Eagle medium (Cambrex Bio Science, Verviers, Belgium, http://www.cambrex.com) + 10% fetal calf serum (Cambrex Bio Science), 100 IU/ml penicillin and 100 μg/ml streptomycin, insulin-transferrin-selenium 1×, retinoic acid 300 ng/ml, linoleic acid 0.8 μg/ml, L-glutamine 2 mM, insulin-like growth factor 1 0.1 ng/ml, and endothelial growth factor 0.1 ng/ml, overnight at 37°C. Such culture medium is hereafter referred to as "complete medium."

Cell Isolation and Purification

The study was performed on female C57/Bl mice (6 weeks old) housed under standard conditions and used under the protocols approved by the institutional Animal Care and Use Committee of the University of Rome Tor Vergata (Rome, Italy).

CPCs were isolated from hearts removed from anesthetized mice. Myocardial tissue was minced and incubated at 4°C overnight with 0.05% trypsin in a solution of 0.02% EDTA in phosphate-buffered saline (PBS). The enzymatic reaction was blocked using trypsin inhibitor (Worthington Biochemical Corporation, Lakewood, NY, http://www.worthington-biochem.com), and the tissue fragments were incubated in collagenase II (1500 U) in Leibovitz medium (Worthington Biochemical Corporation) for 30 minutes at 37°C. Thereafter, the fragments were centrifuged for 10 minutes at 800g. Finally, the pellet was resuspended in complete medium, filtered through a 70-μm cell strainer (Falcon BD, Franklin Lakes, NJ, http://www.bdbiosciences.com), and incubated at 37°C, 5% CO_2. The following day, the medium and the nonadhering fragments were removed and substituted with fresh medium. Subsequently, the medium was changed every other day to remove all cardiomyocytes. After 10–15 days, fibroblastoid cells spontaneously migrated out from the fragments and reached confluence. These nonmyocytic cells (NMCs) were trypsinized and harvested.

Bone marrow stromal cells (MSCs) were obtained as described elsewhere [16]. NMCs and MSCs underwent negative immunomagnetic selection to obtain lineage-negative fractions (Lin^{neg}; Miltenyi Biotec GmbH, Bergisch Gladbach, Germany, http://www.miltenyibiotec.com). Briefly, NMCs and MSCs were incubated with a cocktail of biotin-conjugated monoclonal antibodies (CD5, CD45R [B220], CD11b, anti-Ly-6G [Gr-1], 7–4, and Ter-119) and separated by anti-biotin microbead-conjugated secondary antibody. Stem cell antigen 1-positive ($Sca\text{-}1^{pos}$) and $c\text{-}kit^{pos}$ MSCs and NMCs were obtained by incubating the Lin^{neg} populations with microbead-conjugated antibodies directed against the Sca-1 and c-kit antigens, respectively, according to the manufacturer's instruction (Miltenyi Biotec GmbH). An aliquot of the purified cell subpopulations ($Sca\text{-}1^{pos}$, $Sca\text{-}1^{neg}$, $c\text{-}kit^{pos}$, and $c\text{-}kit^{neg}$) was then stained with anti-biotin PE-conjugated secondary antibody (Miltenyi Biotec GmbH) and analyzed with a flow cytometer (data not shown). Bone marrow- and cardiac-derived Lin^{neg} fractions (Lin^{neg}MSCs and Lin^{neg}NMCs), hereafter referred to as MSCs and CPCs, respectively, and the $Lin^{neg}/Sca\text{-}1^{pos}$ fractions were resuspended in complete medium. Cell density was adjusted at $1.5 \times 10^4/cm^2$.

Cell Counting and Seeding

MSCs and CPCs were seeded on films or scaffolds at the concentration of $3 \times 10^4/cm^2$. After 1, 2, 4, 6, and 8 days of culture, cells were detached using a solution containing trypsin 0.05% in EDTA 0.02%. After stopping the reaction with complete medium, cells were centrifuged for 10 minutes at 800g. The pellet was resuspended in complete medium and Neubauer chamber used to count the cells. Each count was repeated at least three times.

Immunofluorescence

Cells seeded on two-dimensional polymeric films, 3D scaffolds, or chamber slides (Falcon BD) were fixed with 4% paraformaldehyde in PBS for 30 minutes at 4°C, and permeabilized with 0.1% Triton X-100 (Sigma-Aldrich) in PBS for 2 minutes at room temperature. Cells were incubated with tetra-rhodamine-conjugated phalloidin, directed against F-actin (Invitrogen Corp., Carlsbad, CA, http://www.invitrogen.com), MF20 antibody, against all sarcomeric myosins in striated muscles (Developmental Studies Hybridoma Bank, University of Iowa, Iowa City, IA), and antibodies against vinculin, α-sarcomeric actin (α-sarc act), α-actinin (Sigma-Aldrich), ISL1 transcription factor (Islet-1), caveolin 3 (Falcon BD), and Sca-1 (R&D Systems, Minneapolis, http://www.rndsystems.com). The appropriate fluorophore-conjugated secondary antibodies were as follows: fluorescein isothiocyanate (FITC)-labeled or rhodamine-labeled anti-mouse, anti-rabbit, and anti-goat IgG (Vector Laboratories, Ltd., Peterborough, England, http://www.vectorlabs.com). Nuclei were stained with 4′,6′-diamidino-2-phenylindole (DAPI; Sigma-Aldrich). Secondary antibodies in the absence of specific primary antibody were used to exclude the occurrence of unspecific signals. The images were taken using a Leica DMRB microscope equipped with a digital camera or using a Leica TCS SP2 confocal microscope (Leica Instruments, Heidelberg, Germany, http://www.leica.com).

RNA Extraction, Retrotranscription, Semiquantitative Reverse-Transcription–Polymerase Chain Reaction

Total RNA was extracted by TRIZOL Reagent (GIBCO BRL, Gaithersburg, MD, http://www.invitrogen.com). Retrotranscription was carried out with 2 μg of RNA for each sample using reverse transcription (RT) Moloney murine leukemia virus (Invitrogen Corp.) in the presence of random hexamers. Semiquantitative analysis of RNA expression was carried out by RT-polymerase chain reaction (PCR) by comparing the control transcript (glyceraldehyde-3-phosphate dehydrogenase) and the transcript of interest when their amplification was in the exponential phase. PCR products were size-fractionated in 2% agarose gel electrophoresis. For primer sequence, see Table 1.

Western Blot

MSCs and CPCs were lysed in radioimmunoprecipitation assay buffer (150 mM NaCl, 50 mM Tris-HCl [pH 7.4], 1% Nonidet P-40, 0.25% sodium deoxycholate, and 2 mM orthovanadate) and a cocktail of protease inhibitors (Sigma-Aldrich). Cell lysates were centrifuged at 13,000g at 4°C for 15 minutes, and protein content was quantified by Bradford method (Amresco, Inc., Solon, OH, http://www.amresco-inc.com/). Thirty micrograms of the extracts were resolved on 10% SDS-polyacrylamide gel electrophoresis, followed by transfer onto polyvinylidene difluoride filters. Filters were blocked with PBS/bovine serum albumin 3% for 45 minutes at T_R and probed with anti-telomerase reverse transcription (TERT), anti-GATA binding protein 4 (GATA-4) (Santa Cruz Biotechnology, Santa Cruz, CA, http://www.scbt.com), anti-connexin 43 (Sigma-Aldrich), anti-caveolin 3 (Falcon BD), and anti-sarcomeric myosin MF20 antibody (Developmental Studies Hybridoma Bank, University of Iowa) for 2 hours at 4°C. The filters were incubated with horseradish peroxidase-conjugated anti-rabbit, anti-mouse, anti-goat secondary antibody (Vector Laboratories Ltd.), and the signal was detected by enhanced chemiluminescence reaction (ECL; Amersham Biosciences, Milano, Italy, http://www.amersham.com).

Flow Cytometry Analysis

Lin^{neg}MSCs and Lin^{neg}CPCs and $Sca\text{-}1^{neg}$, $Sca\text{-}1^{pos}$, $c\text{-}kit^{neg}$, $c\text{-}kit^{pos}$ fractions obtained by immunomagnetic selection were stained with anti-mouse FITC-conjugated secondary antibody (Vector Lab-

Table 1. Primers used for semiquantitative reverse-transcription–polymerase chain reaction

	Forward	Reverse
c-kit	5′-GCCCTAATGTCGGAACTGAA-3′	5′-TTGCGGATCTCCTCTTGTCT-3′
Sca-1	5′-ACTGTGCCTGCAACCTTGTCTGAGA-3′	5′-GTCCAGGTGCTGCCTCCATT-3′
Islet-1	5′-GCCTCAGTCCCAGAGTCATC-3′	5′-AGAGCCTGGTCCTCCTTCTG-3′
Nestin	5′-TCAAGGGGAGGCCAGGAAGGA-3′	5′-CTGCAGCCCCACTCAAGCCATC-3′
Nucleostemin	5′-GGGAAAAGCAGTGTCATTA-3′	5′-GGGATGGCAATAGTAACC-3′
Nanog	5′-ATGGTCTGATTCAGAAGGGC-3′	5′-TTCACCTTCAAATCACTGGC-3′
TEF-1	5′-AAGCGTCAAGCCCTTTGTG-3′	5′-AAAGGAGCACACTTTGGTGG-3′
MEF-2c	5′-AGCAAGAATACGATGCCATC-3′	5′-GAAGGGGTGGTGGTACGGTC-3′
α-MHC	5′-GGAAGAGTGAGCGGCCATCAAGG-3′	5′-CTGCTGGAGAGGTTATTCCTGG-3′
β-MHC	5′-GCCAACACCAACCTGTCCAAGTTC-3′	5′-TGCAAAGGCTCCAGGTCTGAGGGC-3′
osteocalcin	5′-TCTGACAAACCTTCATGTCC-3′	5′-AAATAGTGATACCGTAGATGCG-3′
ALP	5′-CCATTCCCACGTCTTCACATT-3′	5′-AAGGGCTTCTTGTCTGTGTCACT-3′
GAPDH	5′-CAAGATGGTGAAGGTCGGTGTG-3′	5′-GGGGTAAGCAGTTGTGTCAGGAT-3′

Abbreviations: c-kit, CD117; Sca-1, stem cell antigen 1; TEF-1, transcriptional enhancer factor-1; MEF-2C, myogenic enhancer factor-2C; MHC, myosin heavy chain; ALP, alkaline phosphatase; GAPDH, glyceraldehyde-3-phosphate dehydrogenase.

oratories Ltd.). Nuclei were stained with DAPI and analyzed with FACScalibur flow cytometer (Falcon BD). Incubation with FITC-labeled secondary antibody in the absence of specific primary antibody was used to exclude the occurrence of unspecific signals.

Multipotential Capacity

Cell multipotency was assessed challenging MSCs and CPCs with adipogenic or osteogenic medium (Cambrex Bio Science) for 14 days. The presence of osteo-specific markers was assessed by RT-PCR (for primers sequence, see Table 1), whereas lipid vacuoles were visualized by a fluorescence microscope after cell staining with AdipoRed (Cambrex Bio Science). The number of differentiated cells was quantified using DS software (Delta Sistemi, Rome, Italy, http://www.delta-sistemi.it) in 12 random fields as the number of vacuolized cells versus the total number of DAPI-stained nuclei.

Statistical Analysis

The results are presented as mean ± SEM as derived by the unpaired t test. The differences between values were considered significant when $p < .05$.

RESULTS

Characterization of Mesenchymal and Cardiac Progenitors

The phenotype of Lin^{neg}MSCs and Lin^{neg}CPCs cultured in standard conditions up to the 10th passage was assessed by semiquantitative RT-PCR or Western blot, in comparison with cardiac fibroblasts and the cardiomyocyte cell line heart line 5 (HL-5). Figure 1A shows that both stem cell populations displayed phenotypical features of undifferentiated cells, as demonstrated by the expression of c-kit, Islet-1, Sca-1, nanog, nestin, and nucleostemin, independently of the culture passage, whereas cardiomyocyte-specific markers (α-myosin heavy chain [α-MHC], β-MHC, caveolin 3, sarcomeric myosin, as assessed by MF20 antibody, and GATA 4) were absent or faintly expressed (myocyte enhancer factor-2c [MEF-2c], transcription enhancer factor-1 [TEF-1], connexin 43) only in late passages. However, although expressing similar phenotypes, Lin^{neg}MSCs and Lin^{neg}CPCs displayed a different proliferation rate (Fig. 1B), very likely related to the different expression of telomerase-associated protein mTERT (Fig. 1B, inset). In fact, although the Lin^{neg}MSC number increased approximately 10-fold within a week after isolation, the Lin^{neg}CPC number augmented approximately 70-fold within the same time interval. Subsequently, the progenitors among Lin^{neg} populations were obtained by two subsequent sets of immunomagnetic procedures using Sca-1 and c-kit microbead-conjugated antibodies, and the percentage of Sca-1^{pos}, Sca-1^{neg}, c-kit^{pos}, c-kit^{neg} cells in each preparation was evaluated (Fig. 1C, top). Fluorescence-activated cell sorting analysis demonstrated that, in the Lin^{neg}MSC population, the Sca-1^{pos} cells were prevalent (50%) over the c-kit^{pos} cells (10%), whereas, in the Lin^{neg}CPC population, the Sca-1^{pos} and c-kit^{pos} cells were both approximately 10%, as confirmed by immunofluorescence analysis (Fig. 1C, center). The purity of cell preparations was confirmed by RT-PCR using specific probes against Sca-1 and c-kit (Fig. 1C, bottom). The concomitant expression of Sca-1 and c-kit was detected in 2% Lin^{neg} cells only (data not shown). Finally, Lin^{neg} cell multipotency was assessed upon osteogenic and adipogenic medium challenge: approximately 50% Lin^{neg}MSCs differentiated into adipocytes as opposed to 10% of Lin^{neg}CPCs (Fig. 1D). The adipogenic capacity was also retained by both Lin^{neg}/Sca-1^{neg} and Lin^{neg}/Sca-1^{pos} MSCs and CPCs. Osteogenic differentiation of both cardiac- and bone marrow-derived progenitors was also achieved as confirmed by RT-PCR using osteo-specific primers, such as osteocalcin and alkaline phosphatase (Fig. 1D, lower panel).

These results suggested that the Lin^{neg} fraction of bone marrow stroma and the nonmyocytic portion of the heart contain progenitors expressing stem cell markers at different extents; thus, the present investigation was carried out with Lin^{neg}MSCs and Lin^{neg}CPCs (hereafter referred to as MSCs and CPCs, respectively).

Characterization of the Synthetic Scaffolds

PLLA, PLGA, PCL, and PCL/PLLA (BLEND) polymers were used to fabricate planar nonporous (films) and 3D (scaffolds) structures with square (diameter: 100 μm) or hexagonal (diameter: 134 μm) pores. Scaffolds behaved similarly to a textile: when loaded, their weft was rearranged and the fibers aligned in the direction of the applied load [34]. Since the scaffold mechanical properties could be easily modulated by changing their geometry, the elastic modulus of polymeric films and scaffolds was preliminarily assessed (Fig. 2B). The overall scaffold elastic modulus (Fig. 2C) was an order of magnitude lower than in films made of the same materials. In addition, scaffolds with square grid appeared to be the least stiff, since the hexagonal grid had a higher density of lines and its resistance to deformation was greater. In particular, PLLA scaffolds with square grid displayed an elastic modulus that was approximately 330 KiloPascal (kPa) in the direction considered. Technical limits prevented the

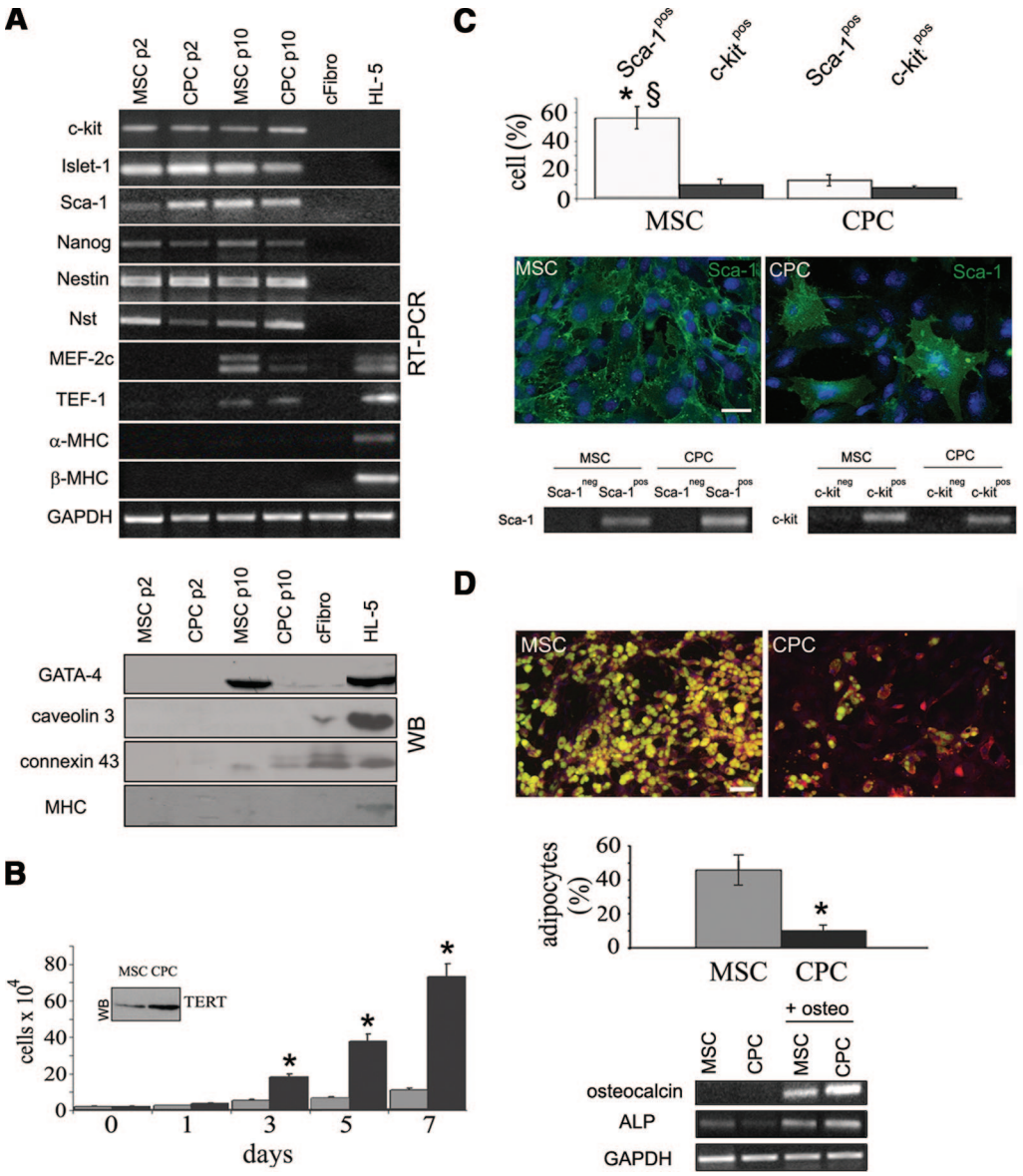

Figure 1. Characterization of MSC and CPC populations. **(A):** Semiquantitative RT-PCR (top) and Western blot (bottom) analyses of the MSC and CPC phenotype. Two different passage times were analyzed for each cell type (MSCs and CPCs): p2 and p10, that is, 1 week and 1 month after cell seeding, respectively. cFIBRO and HL-5 cardiomyocytes were used as controls. RT-PCR signals are specific for: c-kit, Islet-1 (LIM/homeodomain), Sca-1, Nanog, Nestin, Nst, MEF-2c, TEF-1, α-MHC, β-MHC, and GAPDH. Representative Western blot analyses showing the dynamics of several cardiac specific markers: GATA-4, caveolin 3, connexin 43, and MHC. Cell phenotype analysis displays a feeble activation of early cardiac-specific genes and proteins at p10 only. **(B):** MSC (gray) and CPC (black) growth curve in standard culture conditions and TERT protein expression (inset). A remarkable difference in proliferation rate of CPCs in respect to MSCs is detectable. $*$, $p < .001$. **(C):** Sca-1- and c-kit-positive cells (%) within CPC and MSC populations (top). Immunofluorescence analysis of Sca-1 expression (green) in MSCs and CPCs (middle); 4′,6′-diamidino-2-phenylindole nuclei counterstaining (blue). RT-PCR analysis of Sca-1 expression after purification of Sca-1^{neg} and Sca-1^{pos} subpopulations (bottom, left) and c-kit expression in c-kit^{neg} and c-kit^{pos} subpopulations of MSCs and CPCs (bottom, right). A significantly higher percentage of Sca-1^{pos} progenitors is present in MSCs versus CPCs; conversely, no significant difference in c-kit^{pos} cells from both naïve populations is detectable. Data are representative of, at least, six independent experiments performed in triplicate. $*$, $p < .001$, Sca-1^{pos} versus c-kit^{pos} MSCs; §, $p < .001$, Sca-1^{pos} MSC versus Sca-1^{pos} CPCs. **(D):** Immunofluorescence analysis of CPC and MSC adipogenic differentiation, as shown by the presence of intracellular lipid droplets (yellow, top), and percentage of adipocytes differentiated from MSCs and CPCs (center). MSCs are more prone to assume an adipocytic phenotype. Values are derived from eight random fields in each of the five slides analyzed. $*$, $p < .001$. Semiquantitative RT-PCR analysis of osteogenic differentiation of MSCs and CPCs: RT-PCR signals are specific for the osteoblast markers osteocalcin and ALP. Scale bars = 10 μm **(C)**, 25 μm **(D)**. Abbreviations: alpha-MHC, alpha-myosin heavy chain; beta-MHC, beta-myosin heavy chain; ALP, alkaline phosphatase; cFIBRO, cardiac fibroblasts; c-kit, CD117, stem cell factor receptor; CPC, cardiac progenitor cell; GAPDH, glyceraldehydes-3-phosphate dehydrogenase; GATA-4, GATA binding protein 4; HL-5, heart line 5; Islet-1, ISL1 transcription factor; MEF-2c, myocyte enhancer factor-2c; MSC, mesenchymal stem cell; Nanog, homeobox transcription factor; Nestin, intermediate filament gene; Nst, nucleostemin; RT-PCR, reverse-transcription polymerase chain reaction; Sca-1, stem cell antigen 1; TEF-1, transcription enhancer factor-1; TERT, telomerase reverse transcriptase; WB, Western blotting.

experimental assessment of the scaffold elastic modulus in different directions. However, a mathematical model indicated that the elastic modulus for PLLA square grid scaffolds could be in the range of 330–370 kPa (Fig. 6).

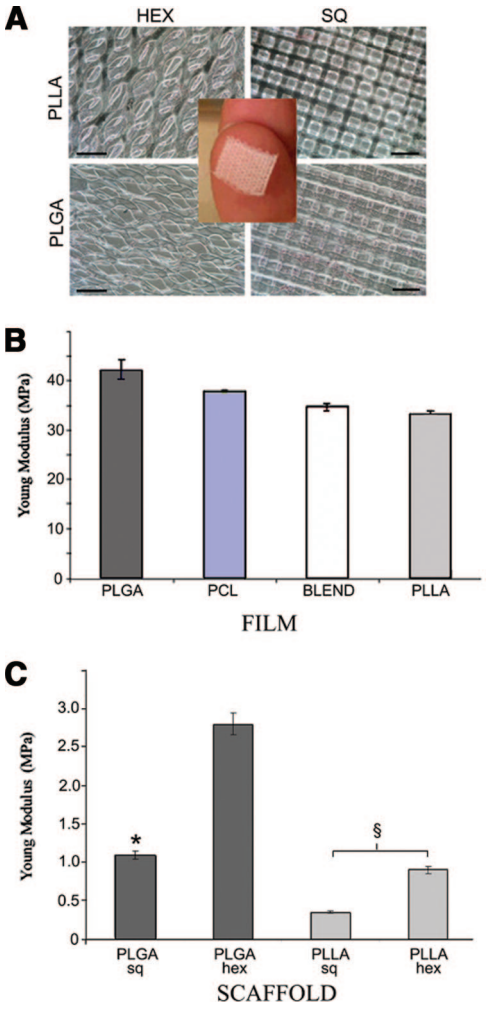

Figure 2. Mechanical characterization of polymeric films (two dimensional [2D]) and scaffolds (three dimensional [3D]). **(A):** Representative micrographs of PLLA and PLGA scaffolds with hex and sq pores. Phase contrast. The central inset shows a macroscopic view of a polymeric 3D scaffold on a human finger. **(B):** Bars are representative of the elastic modulus, expressed as MPa, of 2D polymeric films and **(C)** 3D PLGA and PLLA scaffolds with sq and hex grid. PLLA displays the lowest Young modulus in both polymeric films and scaffolds especially when a square geometry is adopted. *, $p < .001$, square versus hexagonal pores; §, $p < .001$, PLLA versus PLGA. Scale bar = 100 μm. Abbreviations: BLEND, mixture (40:2) of PLGA and PCL; hex, hexagonal; MPa, MegaPascal; PCL, polycaprolactone; PLGA, polyglicolide; PLLA, polylactide; sq, square.

Interfacing MSCs and CPCs with Polymeric Films

The adhesive capacity of MSCs and CPCs on four chemically different polymeric films was calculated as the percentage of cells adhering on the bidimensional structures 24 hours after seeding. Depending on the film chemistry, cell adhesion was highly variable: MSCs were maximally adhering on BLEND (67.0% ± 6.0%), whereas on PCL (42.7% ± 5.3%), PLGA (32.0% ± 4.1%), and PLLA (18.7% ± 2.1%) (Fig. 3A, top) cell ability to interact with the synthetic material was remarkably lower. Conversely, CPCs were maximally adhering on PLGA (33.7% ± 2.8%) and PLLA (30.0% ± 2.2%), whereas only 15.0% ± 1.6% and 17.5% ± 1.9% of cells adhered on PCL and BLEND, respectively (Fig. 3B, top). In addition, MSCs were potently stimulated to proliferate on PLGA and PLLA from day 1 through day 4, but not on PCL and BLEND (Fig. 3A, bottom). In opposition, CPCs displayed a good proliferative response to PLGA and PLLA, whereas they completely failed to proliferate on PCL and BLEND (Fig. 3B, bottom).

Morphological analysis showed that MSCs and CPC, grown as a monolayer, preserved their morphology and proper cytoskeleton organization and function on all the polymeric films considered, as demonstrated by actin and vinculin decoration (Fig. 3C). Moreover, when challenged with differentiative medium, both cell types showed the ability to generate adipocytes on all the polymers tested, demonstrating the persistence of their multipotential attitude (Fig. 3D).

Taken together, preliminary assessments performed on polymeric films suggested to select PLLA and PLGA as the most suitable materials for ensuing experiments on 3D scaffolds.

Biological Response of MSCs and CPCs to 3D Scaffolds with Different Pore Geometry

Progenitor cells were seeded onto sterile 3D scaffolds of PLLA and PLGA (Fig. 4). MSCs and CPCs retained their morphology independently of pore geometry (data not shown), although stem cell ability to adhere to scaffolds was geometry-dependent (Fig. 4A). In fact, 24 hours after seeding on 3D PLGA scaffolds, MSC adhesion was significantly higher in the presence of square (18.5% ± 2.4%) than hexagonal (3.7% ± 0.4%) pores. Conversely, after 24-hour seeding on 3D PLLA scaffolds, MSC adhesion was 7.3% ± 0.8% with square pores and 11.0% ± 1.3% with hexagonal pores (Fig. 4A, upper panel). CPC adhesive response to 3D scaffold geometry paralleled that of MSCs, except for slight differences in cell percentage adhesion (Fig. 4A, lower panel). Indeed, in both cases, the adhesion rate on tridimensional scaffolds was as follows: square PLGA > hexagonal PLLA > square PLLA > hexagonal PLGA. Stem cell adhesion was confirmed by immunofluorescence analysis of the colonized scaffolds (CPCs in Fig. 4B) and the expression of vinculin (Fig. 4C). Similar results were obtained with MSCs (data not shown). Finally, both cell types preserved their multipotential attitude on all the scaffolds tested, as shown when challenged with adipogenic medium (Fig. 4D).

Divergent Behavior of MSCs and CPCs on 3D Scaffolds

After 1- and 2-week culture on 3D scaffolds, cells retaining Sca-1, c-kit, and Islet-1 expression were detectable within MSC population in the absence of differentiative markers (Fig. 5A). Conversely, when grown on 3D PLLA square scaffolds, de novo expression of myosin transcript was detected in clusters of CPCs (Fig. 5B).

Sca-1^{Pos} CPCs Acquire Cardiac Phenotype on 3D PLLA Scaffolds with Square Pores

To clarify the nature of cells prone to adopt the cardiomyocyte phenotype, Sca-1^{pos} CPCs and MSCs were isolated and cultured for 2 weeks on PLLA scaffolds with square pores. Immunofluorescence analysis using cardiac-specific markers, such as sarcomeric myosin (MF-20), α-sarc act, caveolin 3, and actinin confirmed the commitment of the Sca-1^{pos} subset of CPCs (Fig. 5C). Such phenotype and growth behavior were not detectable on PLGA or on PLLA with hexagonal pores (data not shown). Confocal microscopy of committed Sca-1^{pos} CPCs decorated with antibodies directed against cardiac-specific markers showed that cells assumed a characteristic tissue-like architecture on 3D PLLA scaffolds with square pores colonizing even the scaffold inner layers (Fig. 6A, 6B). In fact, on square PLLA scaffolds, cells aligned in a characteristic direction (approximately 45° ± 15° in respect to an arbitrary x-axis, θ angle) (Fig. 6C) corresponding to the areas theoret-

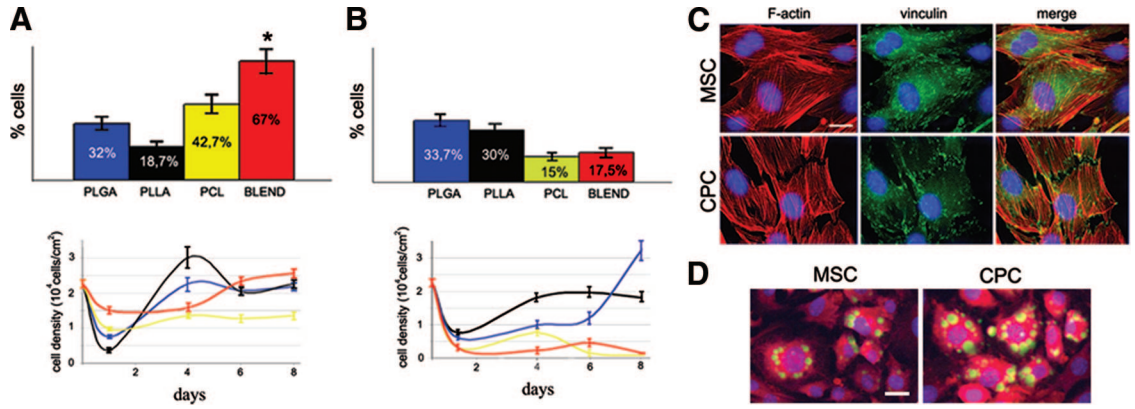

Figure 3. Progenitor cell response to film chemical composition. **(A):** MSC and **(B)** CPC adhesion (top) and proliferation (bottom) ability on PLGA, PLLA, PCL, and BLEND two-dimensional films. The diagram is representative of at least six independent experiments performed in triplicate. *, $p <$ .001, BLEND versus PLGA, PLLA, and PCL. **(C):** MSC and CPC cytoskeletal organization (F-actin, red) and expression of adhesion proteins (vinculin, green) on PLLA films. Equivalent results were obtained after cell seeding on PLGA, PCL, and BLEND films. **(D):** MSCs and CPCs retain multipotency on all the polymers tested (representative pictures of MSC and CPC differentiation on PLLA), as shown by the presence of lipid droplets (yellow) after cell treatment with adipogenic medium. MSCs and CPCs display distinct adhesive and proliferative responses in respect to the film chemical composition. No significant differences in cell adipogenic potential were detected. Scale bars = 10 μm (**C, D**). Abbreviations: BLEND, mixture (40:2) of PLGA and PCL; CPC, cardiac progenitor cell; MSC, mesenchymal stem cell; PCL, polycaprolactone; PLGA, polyglicolide; PLLA, polylactide.

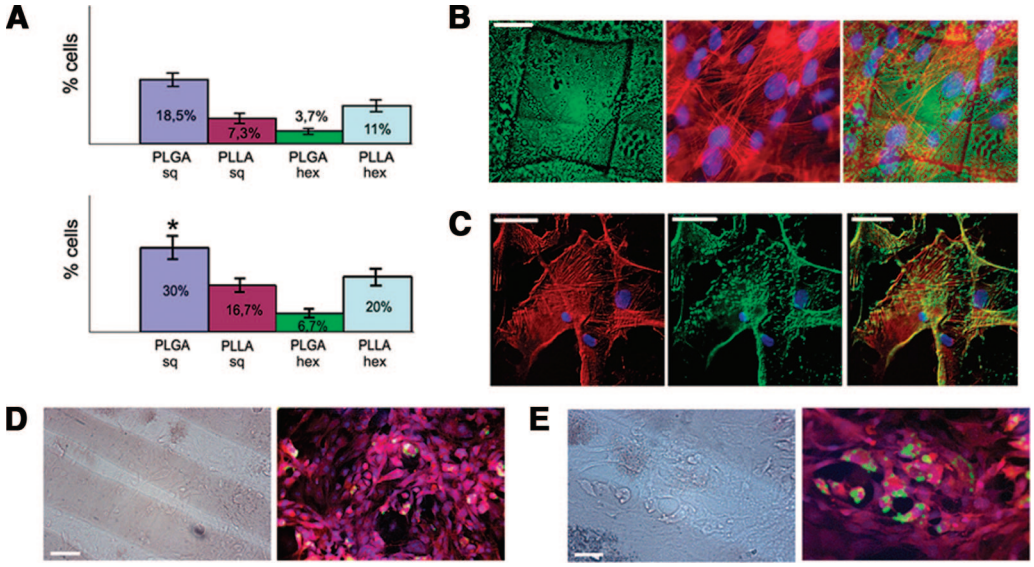

Figure 4. Progenitor cell response to three-dimensional (3D) scaffold geometry and stiffness. **(A):** MSC (top) and CPC (bottom) adhesion fraction on 3D scaffolds, as evaluated 24 hours after cell seeding. The diagram is representative of, at least, six independent experiments performed in triplicate. Immunofluorescence **(B)** and confocal **(C)** image of CPCs exhibiting the expression of F-actin (red), vinculin (green), and related merge (yellow) within square pore PLLA scaffolds. **(D):** Adipocytic differentiation of MSCs and **(E)** CPCs cultured on 3D square PLLA scaffolds. Equivalent results were obtained on the other 3D scaffolds tested. MSCs and CPCs display distinct adhesive ability, while retaining multipotential attitude on all 3D scaffolds evaluated. Scale bars = 25 μm **(B)**, 35 μm **(C)**, 70 μm (**D, E**). *, $p <$ .001, PLGA sq versus PLGA hex, PLLA sq, PLLA hex. Abbreviations: CPC, cardiac progenitor cell; hex, hexagonal; MSC, mesenchymal stem cell; PLGA, polyglicolide; PLLA, polylactide; sq, square.

ically endowed with minor stiffness (Fig. 6D). Such an alignment was not detectable on PLGA or on PLLA with hexagonal pores, whereas MSCs showed random growth on all the polymers tested (Fig. 7).

DISCUSSION

In recent years, contrasting protocols have been proposed to differentiate stem cells into cardiomyocytes in vitro. These protocols shared a few common characteristics, among which the most important was that mainly soluble factors (growth factors or substances acting on epigenetic mechanisms) were used to drive stem cells to commit, express late muscle differentiation markers, assemble the complex sarcomeric machinery, and, ultimately, induce cardiomyocytes to beat [14–16, 20, 23]. Conversely, in vivo studies have been characterized by insisted attempts to demonstrate that diverse stem cell subpopulations can regenerate portions of damaged myocardium after a simple stimulation with a single or a combination of few growth factors [21, 35]. Unfortunately, controlled clinical trials performed administering progenitor cells showed that current stem cell technology does not determine any factual advantage for cardiac patients [2].

The present study demonstrates, as a proof of concept, that stem cell differentiation to cardiomyocytes occurs only when a "critical environment," highly specific for each stem cell subset,

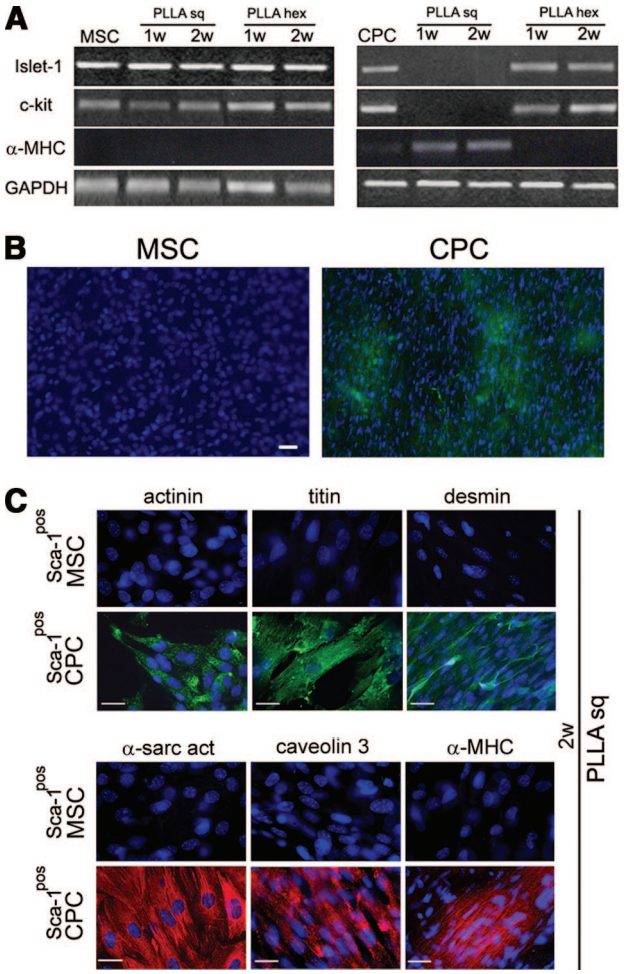

Figure 5. MSC and CPC divergent differentiative potential on three-dimensional (3D) scaffolds. **(A):** Semiquantitative reverse-transcription–polymerase chain reaction analysis of MSCs (left) and CPCs (right) after 1 and 2 w culture on sq and hex PLLA scaffolds. CPC stemness markers are extinguished after 1 week of culture, whereas the cardiac-specific marker α-MHC is expressed. **(B):** Immunofluorescence analysis of MSC (left) and CPC (right) myosin expression. **(C):** Sca-1^{pos} MSC and Sca-1^{pos} CPC differentiation on 3D square PLLA scaffolds. An array of cardiac-specific markers is expressed by Sca-1^{pos} CPCs, but not Sca-1^{pos} MSCs, after 2 week-culture. Scale bars = **(B)** 30 μm, **(C)** 10 μm. Abbreviations: α-sarc act, α-sarcomeric actin; α-MHC, α-myosin heavy chain; CPC, cardiac progenitor cell; hex, hexagonal; MSC, mesenchymal stem cell; PLLA, polylactide; Sca-1^{pos}, stem cell antigen 1-positive; sq, square; w, weeks.

is established by fine-tuning the interaction of soluble and physical factors. This concept was corroborated by comparing the characteristics of two different subsets of multipotent progenitors obtained by different sites (bone marrow and heart) when cultured on scaffolds with defined chemical composition and pore geometry. After excluding that chemical composition and fabrication process could affect cell integrity and function, pore geometry and, above all, the related scaffold stiffness emerged as the crucial factor in driving stem cell differentiation. Experimental data showed that cardiomyocyte phenotype can be elicited, in the presence of the same medium, only when the stiffness of the scaffold is <100 kPa (PLLA with square pores). Furthermore, the differentiating cells adopted a peculiar orientation along the arbitrary 45°± 15° axis of the scaffold (Fig. 6), where the stiffness was constantly maintained <100 kPa. In fact, accurate design and manufacturing procedures allowed modulating the stiffness of the inert structures: the multiwell bottom (polystyrene), the film (35–45 MPa), the three-dimensional hexagonal scaffold (1–3 MPa), and the three-dimensional square scaffold (70–330 kPa) exhibited a progressively decreasing stiffness dictated by the polymer characteristics and structure geometry. In particular, the PLLA scaffold with square geometry displayed an anisotropic rigidity dependent on the direction of the applied force, as predicted by the mathematical model ad hoc developed. No investigations have been carried out so far to establish the optimal scaffold stiffness inducing cardiomyocyte phenotype nor have cardiac progenitors been tested in this respect. Previous studies indicated that the differentiation of myoblasts and MSCs to striated (not cardiac) muscle can be selectively achieved on scaffolds with highly defined stiffness (12 kPa) [29, 34]. In the present investigation, scaffold stiffness inducing cardiomyocyte differentiation was higher in respect to skeletal muscle, very likely, because the passive stiffness, representative of the noncontractile extracellular tissue skeleton, is several fold higher in myocardial [36, 37] versus skeletal muscle tissue, although variable values have been reported using diverse assessment techniques [38, 39]. Therefore, it is likely that stem cells need to sense cardiac extracellular matrix or any other support emulating it to activate the differentiation program. Cell orientation and differentiation could be dictated by the need to stabilize the entire system, balancing the inherent cell tensile force and scaffold stiffness, as stated by the tensegrity laws [40]. However, in view of a potential clinical application, the flogistic effects of the scaffold by-products must be carefully evaluated and possibly prevented by using adequate bio-erodable polymers. Alternatively, tissue bio-substitutes can be fabricated without scaffolds in form of cell sheets, but how the appropriate matrix stiffness could be emulated remains to be established [41]. Nevertheless, the critical environment used in the present investigation as well as the culture conditions reported in previous studies on stem cell differentiation were able to induce the expression of a wide array of sarcomeric proteins, but were incapable to induce their assembly in the final sarcomeric machinery, even when the culture was protracted for 3 weeks. Manifestly, stem cells need some additional still unknown crucial factor to complete cardiomyocyte differentiation.

The effectiveness of the critical environment in inducing a specific phenotype appears to be stem cell specific. In fact, stem cells of different origins do not adopt the same phenotype when challenged with a defined array of soluble and physical factors. In our conditions, progenitor cells have been isolated using standard protocols, purified from lineage-positive contaminants (hematopoietic cells and precursors), and propagated at different growth rates in the absence of spontaneous differentiation events. Moreover, Lin^{neg}MSCs and Lin^{neg}CPCs have been preserved, maintaining the undifferentiated phenotype and multipotency on chemically different polymeric films. Finally, only Lin^{neg}Sca-1^{pos}CPCs committed toward the cardiac phenotype, as witnessed by the expression of specific cardiomyocyte proteins, such as actinin, titin, desmin, α-sarcomeric actin, sarcomeric myosin, and caveolin 3, when cultured on three-dimensional scaffolds having unique fine-tuned pore geometry and dimensions. These results raise interesting questions about the nature of tissue-specific progenitors compared with multipotent mesenchymal progenitors of bone marrow origin. In fact, although sharing many phenotypical features (i.e., stem cell markers), the two Lin^{neg} cell subsets appeared different in cell composition, proliferation rate, and multipotency, and only Lin^{neg}Sca-1^{pos}CPCs were prone to adopt the cardiomyocyte phenotype on PLLA scaffolds with square pores when cultured in the presence of an appropriate medium. Conversely, in the same CPC culturing conditions, MSCs dis-

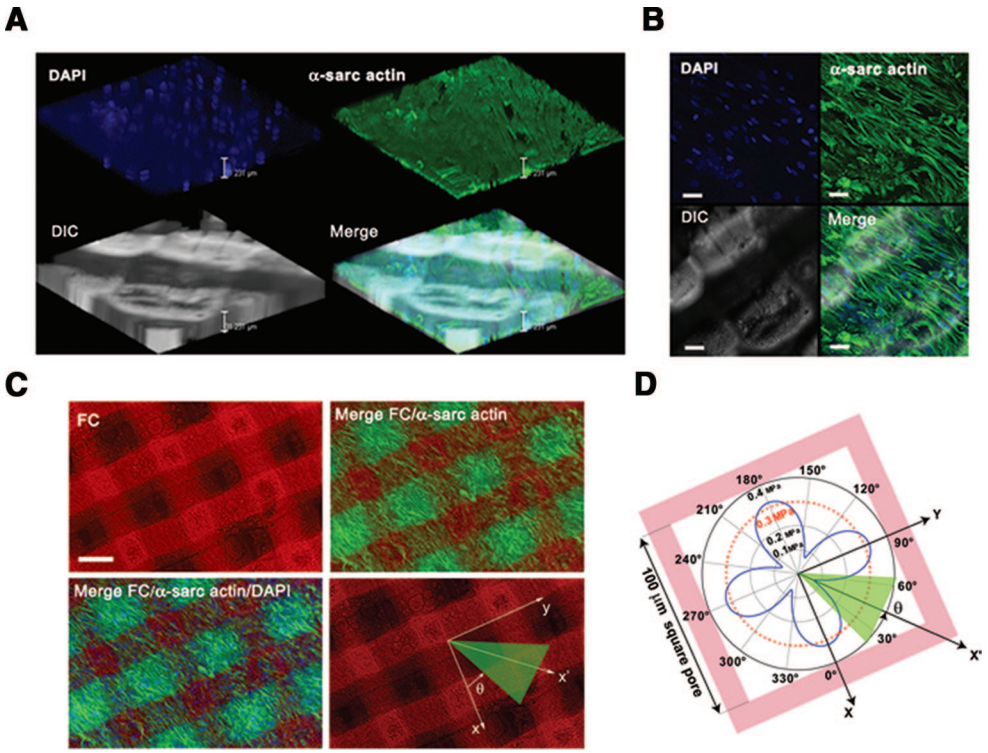

Figure 6. Cardiac progenitor cells (CPCs) differentiate in cardiac proto-tissue on three-dimensional (3D) square polylactide (PLLA) scaffolds. **(A, B):** Confocal images of CPC multilayer colonization of 3D square PLLA scaffolds. **(A):** 3D projection of images taken throughout the thickness of square PLLA scaffold (total thickness: 30.73 ± 4.83 μm). **(B):** Flat 3D reconstruction of images taken throughout the cell monolayer. The image is representative of, at least, six independent experiments. **(C):** Fluorescence micrographs showing the finely regular square grid of PLLA scaffold (phase contrast microscopy, FC), α-sarcomeric actin (α-sarc actin, green hue) of CPC-derived cardiomyocytes on the same scaffold, and DAPI nuclei counterstaining (blue hue). Diagram representative of the CPC cardiomyocyte alignment (green arrows) on the square grid of PLLA scaffolds (bottom right). Newly formed cardiomyocytes are oriented within 10°–20° in respect to an arbitrary *x*-axis paralleling the pores line. **(D):** Anisotropic distribution of the elastic modulus in pore neighborhood, as predicted by a mathematical model (see Materials and Methods section). The pore diagram has the same orientation as the scaffold grid in **(C)**. The predicted stiffness in the green area (10°–20°) approximates the myocardial tissue and corresponds to the actual cell orientation. Scale bars = **(B)** 30 μm, **(C)** 80 μm. Abbreviations: DAPI, 4′,6′-diamidino-2-phenylindole; DIC, interferential contrast acquisition mode.

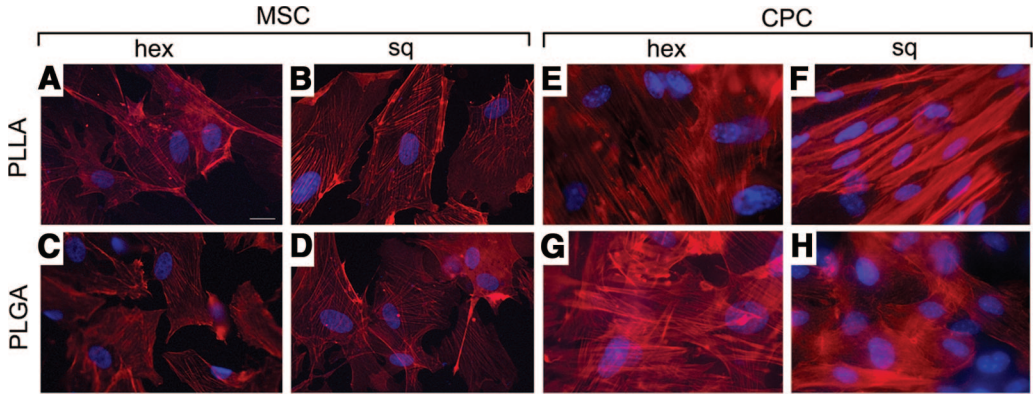

Figure 7. Cardiac progenitor cell (CPC) alignment in fibers on 3D square polylactide (PLLA) scaffolds. Actin staining of MSCs **(A–D)** and CPCs **(E–H)** cultured on sq and hex scaffolds of PLGA and PLLA. Scale bar = 5 μm. Abbreviations: hex, hexagonal; MSC, mesenchymal stem cell; PLGA, polyglicolide; sq, square.

played only faint signals of cardiomyocyte differentiation (MEF-2c, TEF-1 transcripts, and GATA-4 protein), without producing cardiac-specific proteins.

Conclusions

Taken together, these results demonstrate that, as far as stem cell differentiation to cardiomyocytes is concerned, a higher level of complexity with respect to current concepts must be considered and more sophisticated protocols elaborated. In this context, the mechano-structural features of the scaffold are among the major factors in addressing cardiomyocyte phenotype and myocardial organization in vitro, provided that a balanced interaction is established among the mechano-structural features, the stem cell population, and the biological factors within the medium. This implies that, in each organ, at least two different types of niches must be considered: native niches, where inherently unstable (multipotent) stem cells are maintained in a quiescent status, and

differentiating niches, protempore activated tiny regions of the organ where natural stem cell instability is governed in favor of the acceptance of the required phenotype. The present results envisage the feasibility of guiding cardiac differentiation of specifically prone stem cells by replicating in vitro the complex array of signals featuring the original tissue differentiating niche. The conditions characterizing the myocardium-like niches have been identified after a complex series of preliminary experimental sets in which $Lin^{neg}Sca\text{-}1^{pos}$CPCs have been cultured in different environments, all featured by the use of the same cell population, growth medium, multiwell dishes, and inert support materials, to avoid potentially uncontrolled confounding signals, such as those released by natural matrices [30].

These results also entail that novel strategies should be formulated to transplant stem cells in vivo. In this respect, this study paves the way for the ex vivo fabrication of efficient engineered tissues to be engrafted into damaged hearts. In fact, the fine-tuned manipulation of the chemical composition as well as of the geometry and stiffness anisotropy can be exploited to manufacture scaffolds with functionally discrete domains addressing adult stem cells to different phenotype and harmoniously complying with the diverse requirements of vascular versus parenchymal cells. On the other hand, the identification of innovative materials and techniques to fabricate scaffolds complying with the characteristics of the target tissue are prerequisite to the extensive and efficient use of stem cells in clinical practice.

ACKNOWLEDGMENTS

The authors acknowledge the Italian Institute for Cardiovascular Research (INRC) and Compagnia San Paolo (Torino, Italy) for financially supporting this research. M.M. and P.D.N. contributed equally to this work.

DISCLOSURE

The authors indicate no potential conflicts of interest.

REFERENCES

1 Pasumarthi KB, Field LJ. Cardiomyocyte cell cycle regulation. Circ Res 2002;90:1044–1050.
2 Menasche P. Cell transplantation in myocardium. Ann Thorac Surg 2003;75:S20–S28.
3 Murry CE, Field LJ, Menasche P. Cell-based cardiac repair: Reflections at the 10-year point. Circulation 2005;112:3174–3183.
4 Leor J, Amsalem Y, Cohen S. Cells, scaffolds, and molecules for myocardial tissue engineering. Pharmacol Ther 2005;105:151–163.
5 Langer R, Vacanti JP. Tissue engineering. Science 1993;260:920–926.
6 Fan H, Hu Y, Zhang C, Li X et al. Cartilage regeneration using mesenchymal stem cells and a PLGA-gelatin/chondroitin/hyaluronate hybrid scaffold. Biomaterials 2006;27:4573–4580.
7 Yoneno K, Ohno S, Tanimoto K et al. Multidifferentiation potential of mesenchymal stem cells in three-dimensional collagen gel cultures. J Biomed Mater Res 2005;75:733–741.
8 Zimmermann WH, Melnychenko I, Eschenhagen T. Engineered heart tissue for regeneration of diseased hearts. Biomaterials 2004;25:1639–1647.
9 Petite H, Viateau V, Bensaid W et al. Tissue-engineered bone regeneration. Nat Biotech 2000;18:959–963.
10 Cao Y, Vacanti JP, Paige KT et al. Transplantation of chondrocytes utilising a polymer-cell construct to produce tissue engineered cartilage in the shape of a human ear. Plast Reconstruct Surg 1997;100:297–302.
11 Nishida K, Yamato M, Hayashida Y et al. Corneal reconstruction with tissue-engineered cell sheets composed of autologous oral mucosal epithelium. N Eng J Med 2004;351:12–18.
12 Banta MN, Kirsner RS. Modulating diseased skin with tissue engineering: Actinic purpura treated with Apligraf®. Dermatol Surg 2002;28:1103–1106.
13 Bianco P, Riminucci M, Gronthos S, Robey PG. Bone marrow stromal stem cells: nature, biology, and potential applications. STEM CELLS 2001;19:180–192.
14 Makino S, Fukuda K, Miyoshi S et al. Cardiomyocytes can be generated from marrow stromal cells in vitro. J Clin Invest 1999;103:697–705.
15 Xaymardan M, Tang L, Zagreda L et al. Platelet-derived growth factor-AB promotes the generation of adult bone marrow-derived cardiac myocytes. Circ Res 2004;94:E39–E45.
16 Forte G, Minieri M, Cossa P et al. Hepatocyte growth factor effects on mesenchymal stem cells: proliferation, migration, and differentiation. STEM CELLS 2006;24:23–33.
17 Beltrami AP, Cesselli D, Bergamin N et al. Multipotent cells can be generated in vitro from several adult human organs (heart, liver and bone marrow) Blood 2007;110:3438–3446.
18 Messina E, De Angelis L, Frati G et al. Isolation and expansion of adult cardiac stem cells from human and murine heart. Circ Res 2004;95:911–921.
19 Fiaccavento R, Carotenuto F, Minieri M et al. Stem cell activation sustains hereditary hypertrophy in hamster cardiomyopathy. J Pathol 2005;205:397–407.
20 Rosenblatt-Velin N, Lepore MG, Cartoni C et al. FGF-2 controls the differentiation of resident cardiac precursors into functional cardiomyocytes. J Clin Invest 2005;115:1724–1733.
21 Urbanek K, Rota M, Cascapera S et al. Cardiac stem cells possess growth factor-receptor systems that after activation regenerate the infarcted myocardium, improving ventricular function and long-term survival. Circ Res 2005;97:663–673.
22 Oh H, Bradfute SB, Gallardo TD et al. Cardiac progenitor cells from adult myocardium: Homing, differentiation, and fusion after infarction. Proc Natl Acad Sci U S A 2003;14:12313–12318.
23 Matsuura K, Nagai T, Wada H et al. Adult cardiac Sca-1-positive cells differentiate into beating cardiomyocytes. J Biol Chem 2004;279:11384–11391.
24 Hsu S, Chang SH, Yen HJ et al. Evaluation of biodegradable polyesters modified by Type II collagen and Arg-Gly-Asp as tissue engineering scaffolding materials for cartilage regeneration. Artif Organs 2006;30:42–55.
25 Athanasiou KA, Niederauer GG, Agrawal CM. Sterilization, toxicity, biocompatibility and clinical applications of polylactic acid/polyglycolic acid copolymers. Biomaterials 1996;17:93–102.
26 Vozzi G, Previti A, De Rossi D et al. Microsyringe based deposition of 2 and 3-D polymer scaffolds with a well defined geometry for application to tissue engineering. Tissue Eng 2002;8:1089–1098.
27 Cohen S, Bano MC, Cima LG et al. Design of synthetic polymeric structures for cell transplantation and tissue engineering. Clin Mater 1993;13:3–6.
28 Cima LG, Vacanti JP, Vacanti C et al. Tissue engineering by cell transplantation using degradable polymer substrates. J Biomech Eng 1991;113:143–145.
29 Engler AJ, Sen S, Sweeney HL et al. Matrix elasticity directs stem cell lineage specification. Cell 2006;126:677–689.
30 Boontheekul T, Hill EE, Kong HJ et al. Regulating myoblast phenotype through controlled gel stiffness and degradation. Tissue Eng 2007;13:1431–1442.
31 Alperin C, Zandstra PW, Woodhouse KA. Polyurethane films seeded with embryonic stem cell-derived cardiomyocytes for use in cardiac tissue engineering applications. Biomaterials 2005;26:7377–7386.
32 Jager M, Feser T, Denck H et al. Proliferation and osteogenic differentiation of mesenchymal stem cells cultured onto three different polymers in vitro. Ann Biomed Eng 2005;33:1319–1332.
33 Mariani M, Rosatini F, Vozzi G et al. Characterization of tissue-engineered scaffolds microfabricated with PAM. Tissue Eng 2006;12:547–557.
34 Engler AJ, Griffin MA, Sen S et al. Myotubes differentiate optimally on substrates with tissue-like stiffness: Pathological implications for soft or stiff microenvironments. J Cell Biol 2004;166:877–887.
35 Agbulut O, Mazo M, Bressole C et al. Can bone marrow-derived multipotent adult progenitor cells regenerate infarcted myocardium? Cardiovasc. Res 2006;72:175–183.
36 Hidalgo-Bastida LA, Barry JJA, Everitt NM et al. Cell adhesion and mechanical properties of a flexible scaffold for cardiac tissue engineering. Acta Biomater 2007;3:457–462.
37 de Beer EL, Bottone AE, van Der Velden J et al. Doxorubicin impairs

crossbridge turnover kinetics in skinned cardiac trabeculae after acute and chronic treatment. Mol Pharmacol 2000;57:1152–1157.
38 Lieber SC, Aubry N, Pain J et al. Aging increases stiffness of cardiac myocytes measured by atomic force microscopy nanoindentation. Am J Physiol Heart Circ Physiol 2004;287:645–651.
39 Rehfeldt F, Engler AJ, Eckhardt A et al. Cell responses to the mechanochemical microenvironment—Implications for regenerative medicine and drug delivery. Advanced Drug Delivery Reviews 2007;59:1329–1339.
40 Ingber DE. Cellular mechanotransduction putting all the pieces together again. FASEB J 2006;20:811–827.
41 Shimizu T, Yamato M, Kikuchi A et al. Cell sheet engineering for myocardial tissue reconstruction. Biomaterials 2003;24:2309–2316.